

Super-Twisting Sliding Mode Control of DC Microgrids Involving Renewable Sources and Storage Devices

Nasim Ullah*, Asier Ibeas**,***, Abdulrahman Jamal Babqi*, Hend I Alkhamash*, Ahmed Althobaiti*

* *Department of Electrical Engineering, College of Engineering, Taif University, Al-Hawiyah, Taif P.O. Box 888, Saudi Arabia (e-mail: {nasimullah, ajbabqi, khamash.h, ahmed.althobaiti}@tu.edu.sa)*

** *Department of Telecommunications and Systems Engineering, Faculty of Engineering, Universitat Autònoma de Barcelona, 08193 Bellaterra (Cerdanyola del Vallès), Barcelona, Spain (e-mail: asier.ibeas@uab.cat)*

*** *Facultad de Ciencias Económicas y Administrativas, Universidad de Bogotá Jorge Tadeo Lozano, 110311 Bogotá DC, Colombia*

Abstract: This paper describes the application of chattering-free super-twisting sliding mode controllers to the control of DC electric microgrids encompassing renewable sources of energy and storage devices. The microgrid is composed of a photovoltaic source, a super capacitor and a battery set aimed at providing power when the renewable source is not available. These components are connected to a bus by means of DC converters, being each one controlled by the corresponding duty cycle. Three control commands are thus needed to be designed. Moreover, the controller of the DC converter connecting the super capacitor to the bus is designed as a combination of super-twisting and backstepping techniques. This approach combines the simplicity of backstepping designs along with the robustness properties of super-twisting sliding mode controllers. The proposed approach can guarantee the regulation of system's outputs, namely the tracking of the maximum power point, the management of the power provided/absorbed by the battery and the voltage in the bus regardless the presence of potentially time-varying resistive loads. A sensitivity analysis is performed to highlight the effect of control parameters in the closed-loop performance while the effect of time-varying loads and parametric uncertainty is also assessed.

Keywords: DC microgrid, renewable energy, super-twisting sliding-mode control, backstepping.

1. INTRODUCTION

A microgrid (MG) is a small-scale power system aimed at providing the electric supply in an independent way to nearby customers. Thus, three are the main characteristics of a MG: it is local, it is independent, and it is smart. In this way, a MG integrates the energy generators along with the consumers and the control units. In order to reduce the environmental footprint of the generation, the electric power is mainly obtained nowadays by means of renewable energies (RE) such as photovoltaic, wind or sea waves among others (Alharbi et al., 2020; Alzain et al., 2021). The stochastic nature of renewable energy sources, which does not ensure the timely availability of energy, obligates to also include in the system a sort of energy storage (battery bank, supercapacitor, etc.) so that the MG can supply the necessary electric fluid when needed. Consequently, the MG is in the need of a control system able to manage the integration of sources and storage devices as well as to deal with time-varying loads.

Microgrids can be classified into Alternating Current (AC), Direct Current (DC) or hybrid (a combination of AC and DC) ones, (Han et al., 2018; Stojic, 2021). In contrast to AC grids, DC ones offer some advantages such as a simpler structure that leads to a simpler control, less losses (lack of skin effect and less corona loss), and easiness of integration and installation. Therefore, much effort is currently being devoted to the study of DC microgrids, (Han et al., 2018; Weng et al., 2019; Zhang

L. et al., 2019; Zhang Q. et al., 2019; Abdali et al., 2020; Alharbi et al., 2020).

Despite the number of control strategies developed for AC microgrids is large (Kim et al., 2011; Cai et al., 2016; Badal et al., 2019; Sarkar et al., 2020), these cannot be directly applied to DC microgrids due to the different dynamics characterizing both types of systems. Therefore, new control algorithms must be designed for DC grids. In particular, it is of importance the stabilization of the DC link voltage, which represents a daunting challenge due to the nonlinear and coupled dynamics of the whole system. In this way, linear controllers have been employed in (Kumar et al., 2015), robust H_∞ controllers in (Mohammed et al., 2012), droop (Han et al., 2015) and adaptive droop control (Lu et al., 2014) and feedback linearization (Cupelli et al., 2014), to cite just a few. Special attention has been devoted in the literature to nonlinear methods based on Sliding Mode Control (SMC). The main reason for this is that MGs often exhibit a time-varying behavior, uncertainties such as parameter mismatch, and unmodeled dynamics that complicate the efficient operation of the microgrid while a robust control approach is needed to cope with these situations. Hence, since the beginnings of Sliding Mode Control (Itkis, 1976; Utkin, 1977) it has been one of the most extended techniques used to design robust controllers (Gambhire et al., 2021) and it has also been applied to DC microgrids and power systems (Setyawan et al., 2014). Thus, (Cucuzzella et al., 2018) propose a second order sliding

mode controller for the voltage control of boost converters in DC microgrids and (Han et al., 2018) present a higher-order sliding mode control to improve the robustness of islanded and grid-connected operations of a DC microgrid subject to uncertainty. The sliding gain is tuned by means of an adaptive algorithm that provides an automatic procedure to set its value. Furthermore, in (Mobayen et al., 2021) a robust controller based on adaptive sliding-mode techniques is designed for DC-DC buck converters while in (Zhang and Wang, 2017) the adaptive classical sliding mode control is applied to the bus voltage control problem of the equivalent topology (order two) of an islanded DC microgrid.

In addition, chattering has been one of the most well-known concerns of SMC controllers. The presence of high-frequency oscillation in the control signal generates undesirable oscillation in the output, that degrades the performance of the whole system. Therefore, huge efforts have been devoted in the last years to avoid chattering in SMC (Cho and Kerschen, 2016) being the Super-twisting SMC one of the most successful. Thus, (Zeb et al., 2020) design a Super-twisting SMC for a grid-connected photovoltaic system while (Pati and Sahoo, 2017) propose an adaptive approach to the Super-Twisting SMC of a differential boost inverter-based photovoltaic system. Moreover, (Alharbi et al., 2020; Sami et al., 2020a; Sami et al., 2020b; Ullah, 2020) apply the fractional counterpart of Super-twisting sliding mode controllers to deal with the control problem of DC microgrids. Super-twisting sliding mode controllers have a well-established theory developed during the last years for both SISO and MIMO systems (Emelyanov et al., 1996; Levant, 2001; Mondal and Mahanta, 2013; Moreno, 2014, Nagesh and Edwards, 2014; Jouini et al., 2017; Feng and Fei, 2018; Svecko et al., 2020), to cite just a few.

This paper applies a Super-Twisting Sliding Mode Controller (ST-SMC) to a high-order multivariable DC microgrid to solve the voltage control problem regardless the presence of a time-varying load in the system. The system is composed of a photovoltaic source along with a supercapacitor and a battery. A capacitor, whose voltage will be controlled, is also added on the source side (Iovine et al., 2017). In addition, a generalization of the approach of (Nagesh and Edwards, 2014) is adopted for which a general super-twisting exponent p is considered while a general structure for the regulation mechanism (in the sense of Jouini et al., 2017) is employed to enhance the convergence and robustness properties of the controller. Furthermore, the design of the control command corresponding to the super capacitor is performed by combining the backstepping and ST-SMC techniques. As it is shown in (Shen et al., 2019) this approach merges the simplicity of the backstepping control design while retaining the robustness properties of the ST-SMC. In this way, the main contributions of the work can be summarized as the design of a general ST-SMC with arbitrary super-twisting exponent and regulation equation, combined with backstepping and applied to a multi-variable high-order nonlinear DC microgrid composed of RE sources and storage devices, and feeding time-varying loads. A combination of higher-order and super-twisting sliding-mode controllers is

used in (Tayebi-Haghighi et al., 2018) to design a robust chattering-free controller for robotic manipulators. This approach differs from the one adopted in this work, which is based on the combination of super-twisting and backstepping techniques. To the best of authors' knowledge, this is the first time that this control method has been applied to the studied system. Therefore, the description of the control law along with simulation examples of the obtained performance and influence of parameters are discussed in this work.

The rest of the paper is organized as follows. Section 2 describes the DC microgrid model and presents the problem to be solved. The control algorithm is introduced in Section 3. Section 4 contains the simulation results obtained for the controller and the robustness and sensitivity analysis. Finally, conclusions end the paper.

2. MODEL DESCRIPTION AND CONTROL OBJECTIVE

The DC microgrid model is taken from (Abdali et al., 2020) which in turn is adopted from (Iovine et al., 2017) and represents a common architecture for DC microgrids (Zhang Q. et al., 2019). Therefore, the proposed control strategy is newly applied to a benchmark case study. The DC microgrid is composed of a photovoltaic source that supplies energy to a potentially time-varying DC load (R_L) and uses a battery and a capacitor bank storage to provide energy when the RE photovoltaic source is not available. DC-DC converters are employed to couple the source and storage devices to the DC bus. This system is represented in Figure 1, where the capacitor C_9 is also considered. By taking the state variables as $x_1 = v_{C_1}$, $x_2 = v_{C_2}$, $x_3 = I_{L_3}$, $x_4 = v_{C_4}$, $x_5 = v_{C_5}$, $x_6 = I_{L_6}$, $x_7 = v_{C_7}$, $x_8 = I_{L_8}$, $x_9 = v_{C_9}$, the mathematical description of the model (by using the averaging technique) is given by Equations (1)-(9), (Iovine et al., 2017). It is important to point out that this model is of dimension nine, which is higher than previous models used in the literature to test the ST-SMC controllers, (Jouini et al., 2017).

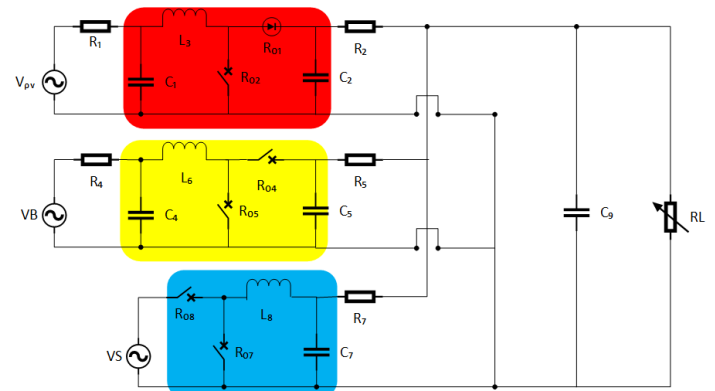


Fig. 1. DC microgrid considered for control (Iovine et al., 2017; Abdali et al., 2020).

$$\dot{x}_1 = -\frac{1}{R_1 C_1} x_1 - \frac{1}{C_1} x_3 + \frac{1}{R_1 C_1} V_{PV} \quad (1)$$

$$\dot{x}_2 = -\frac{1}{R_2 C_2} x_2 + \frac{1}{C_2} x_3 - \frac{1}{C_2} u_1 x_3 + \frac{1}{R_2 C_2} x_9 \quad (2)$$

$$\dot{x}_3 = \frac{1}{L_3} (x_1 - x_2 - R_{01} x_3) + \frac{1}{L_3} (x_2 + (R_{01} - R_{02}) x_3) u_1 \quad (3)$$

$$\dot{x}_4 = -\frac{1}{R_4 C_4} x_4 - \frac{1}{C_4} x_6 + \frac{1}{R_4 C_4} V_B \quad (4)$$

$$\dot{x}_5 = -\frac{1}{R_5 C_5} x_5 + \frac{1}{C_5} x_6 - \frac{1}{C_5} u_2 x_5 + \frac{1}{R_5 C_5} x_9 \quad (5)$$

$$\dot{x}_6 = \frac{1}{L_6} (x_4 - x_5 - R_{04} x_6 + u_2 x_5) \quad (6)$$

$$\dot{x}_7 = -\frac{1}{R_7 C_7} x_7 + \frac{1}{C_7} x_8 + \frac{1}{R_7 C_7} x_9 \quad (7)$$

$$\dot{x}_8 = \frac{1}{L_8} (u_3 V_S - R_{08} x_8 - x_7) \quad (8)$$

$$\dot{x}_9 = \frac{1}{C_9} \left(\frac{x_2 - x_9}{R_2} + \frac{x_5 - x_9}{R_5} + \frac{x_7 - x_9}{R_7} - \frac{x_9}{R_L} \right) \quad (9)$$

The three control inputs given by u_1, u_2, u_3 , which represent the duty cycles of each of the DC converters, must satisfy the constraint $0 \leq u_1, u_2, u_3 \leq 1$. R_L denotes the potentially time-varying resistive (DC) load. The control signal u_1 aims at integrating the energy coming from the photovoltaic source and, simultaneously, to track the maximum power point. Therefore, u_1 is employed to force x_1 to track its reference x_1^* corresponding to the Maximum Power Point Tracking (MPPT). This reference value is provided by a higher-level controller which will not be considered in this paper so that the value of x_1^* is assumed to be known in this work. There are several MPPT algorithms that can be used for this purpose (see, for instance, (Tobon et al., 2020) and the references therein for more information on MPPT algorithms). The control signal u_2 is aimed at forcing x_4 to track its specified reference value x_4^* regulating the amount of power provided or absorbed by the battery. This reference value is also specified by a higher-level controller that determines it with the aim of maximizing its lifetime. It will be assumed that this value is also known and constant in this work. Finally, the control signal u_3 can be used to control the variable x_7 corresponding to the supercapacitor voltage connected to the grid. However, in order to guarantee the stability of the DC bus voltage, u_3 will be employed to control the voltage drop at capacitor C_9 , which is given by x_9 . This fact implies that the system is not fully controllable and the variable x_7 will no longer be controlled. A backstepping approach along with the ST-SMC will be employed to control the x_9 variable to its reference constant desired value of x_9^* . It will be assumed along this work that the input voltages, V_{PV}, V_B, V_S and the state values are measured, and are consequently known, the parameters of the DC converters are known, and the resistive load may be unknown and time-varying in the general case (Iovine et al., 2017). These assumptions are feasible with the practical use of the system. The equilibrium point desired for this system is represented by:

$$x_e = \left[x_1^* \ x_2^* \ x_3^* \ x_4^* \ x_5^* \ x_6^* \ x_7^* \ x_8^* \ x_9^* \right]^T \quad (10)$$

where the values of x_7^*, x_8^* will be calculated below according to a backstepping procedure since the control objective is replaced by controlling x_9 instead of x_7 . Furthermore, the equilibrium point must satisfy the following relations (11)-(15) for x_2^* and x_5^* (Iovine et al., 2017):

$$\Delta_2 = \frac{1}{R_1 C_2} (V_{PV} - x_1^*) \left[x_1^* - \frac{R_{02}}{R_1} (V_{PV} - x_1^*) \right] \quad (11)$$

$$\Delta_2 = \frac{1}{R_4 C_5} (V_B - x_4^*) \left[x_4^* - \frac{R_{04}}{R_4} (V_B - x_4^*) \right] \quad (12)$$

$$\alpha = \frac{R_{01} - R_{02}}{R_1} (V_{PV} - x_1^*) \quad (13)$$

$$x_2^* = \frac{x_9^* - \alpha}{2} + \frac{1}{2} \sqrt{(x_9^* - \alpha)^2 + 4R_2 C_2 (\Delta_2 + \alpha x_9^*)} \quad (14)$$

$$x_5^* = \frac{x_9^*}{2} + \frac{1}{2} \sqrt{(x_9^*)^2 + 4R_5 C_5 \Delta_5} \quad (15)$$

The next Section 3 addresses the design of the control commands to achieve the objectives described before.

3. CONTROLLER DESIGN

Each of the control laws u_1, u_2, u_3 , is designed separately to fulfill the objectives described in Section 2. Thus, the first control command u_1 is designed as follows based on the super-twisting approach of (Nagesh and Edwards, 2014) with some generalizations. Initially, the error control signal is defined as $\sigma_i = x_i - x_i^*$ for $i = 1, 2, \dots, 9$. The function σ is usually referred to as the sliding surface in the sliding mode control literature (Gambhire et al., 2021). The controller is formulated as:

$$u_1 = \frac{L_3}{x_2 + (R_{01} - R_{02})x_3} \left(-\frac{x_1}{L_3} + \frac{x_2}{L_3} + \frac{R_{01}}{L_3} x_3 + v_1 + \dot{x}_3^* \right) \quad (16)$$

$$v_1 = -k_{11} \text{sign}(\sigma_3) |\sigma_3|^p - k_{21} \sigma_3 + z_1 \quad (17)$$

$$\dot{z}_1 = -k_{31} \text{sign}(\sigma_3) - k_{41} (1 - \delta) \sigma_3 - \delta k_{51} z_1, \quad z_1(0) = 0 \quad (18)$$

where \dot{x}_3^* stands for the derivative of the reference target, which is known since it is specified by the designer beforehand (being zero when x_3^* is constant), $\delta \in \left\{ 0, \frac{1}{2}, 1 \right\}$ selects the type of regulation equation (18) employed, $(0 < p < 1)$ is the super-twisting index and $k_{j1} > 0$ are positive gains for $j = 1, 2, \dots, 5$. It is remarkable to point out here that in this work we consider a more general equation (18) than in (Nagesh & Edwards, 2014), applied to the control of the proposed DC microgrid. The above controller (16)-(18) renders the closed-loop for the x_3 variable to:

$$\dot{\sigma}_3 = \dot{x}_3 - \dot{x}_3^* = -k_{11} \text{sign}(\sigma_3) |\sigma_3|^p - k_{21} \sigma_3 + z_1 \quad (19)$$

It is proved in (Moreno, 2014) that an appropriate choice for the positive gains k_{j1} allows ensuring $x_3 \rightarrow x_3^*$, which in turn ensures that $x_1 \rightarrow x_1^*$ according to the definition of the equilibrium point (10) and dynamic equation (1). Consequently, the proposed controller can successfully achieve the control objective set up for u_1 , that is the tracking of the maximum power point. The second control law, u_2 , is designed as:

$$u_2 = \frac{L_6}{x_5} \left(-\frac{x_4}{L_6} + \frac{x_5}{L_6} + \frac{R_{04}}{L_6} x_6 + v_2 + \dot{x}_6^* \right) \quad (20)$$

$$v_2 = -k_{12} \text{sign}(\sigma_6) |\sigma_6|^p - k_{22} \sigma_6 + z_2 \quad (21)$$

$$\dot{z}_2 = -k_{32} \text{sign}(\sigma_6) - k_{42} (1 - \delta) \sigma_6 - \delta k_{52} z_2, \quad z_2(0) = 0 \quad (22)$$

where \dot{x}_6^* stands for the derivative of the reference target, which is known since it is specified by the designer beforehand, $\delta \in \left\{ 0, \frac{1}{2}, 1 \right\}$ selects the type of regulation

equation (22) employed, which is the same value as in (18), (i.e., the signal δ is shared by all controllers) and $k_{j2} > 0$ are positive gains for $j = 1, 2, \dots, 5$. Likewise, the controller (20)-(22) renders the closed-loop for the x_6 variable to:

$$\dot{\sigma}_6 = \dot{x}_6 - \dot{x}_6^* = -k_{12} \text{sign}(\sigma_6) |\sigma_6|^p - k_{22} \sigma_6 + z_2 \quad (23)$$

for which an appropriate choice for the positive gains k_{j2} allows ensuring $x_6 \rightarrow x_6^*$, which in turn ensures that $x_4 \rightarrow x_4^*$ according to the definition of equilibrium point (10) and dynamic equation (4). Consequently, the proposed controller successfully achieves the control objective set up for u_2 that is the regulation of the amount of power provided or absorbed by the battery.

The design of u_3 is more elaborate since it will be dedicated to control x_9 instead of x_7 . Therefore, the backstepping approach employed in (Iovine et al., 2017) will be adopted. In this way, initially the value of x_7 will be used as virtual input. Then, in order to achieve the desired value for x_7 (denoted by x_7^*), the desired value for x_8 will be calculated and, finally, u_3 is designed to force x_8 to track its calculated reference x_8^* . To this end, the Lyapunov function candidate $V_9 = \frac{C_9}{2} (x_9 - x_9^*)^2$ is proposed. Its time derivative is given by:

$$\begin{aligned} \dot{V}_9 &= C_9 \dot{x}_9 (x_9 - x_9^*) \\ &= \left(\frac{x_2 - x_9}{R_2} + \frac{x_5 - x_9}{R_5} + \frac{x_7 - x_9}{R_7} - \frac{x_9}{R_L} \right) (x_9 - x_9^*) \end{aligned}$$

The variable x_7 is used as virtual input to render the above equation into:

$$\dot{V}_9 = C_9 \dot{x}_9 (x_9 - x_9^*) = -K_9 (x_9 - x_9^*)^2 \leq 0$$

with $K_9 > 0$ by setting:

$$\frac{x_2 - x_9}{R_2} + \frac{x_5 - x_9}{R_5} + \frac{x_7 - x_9}{R_7} - \frac{x_9}{R_L} = -K_9 (x_9 - x_9^*)$$

Thus, x_7 should track the desired value x_7^* given by:

$$x_7^* = R_7 \left[-\frac{x_2}{R_2} - \frac{x_5}{R_5} - K_9 (x_9 - x_9^*) + \left(\frac{1}{R_2} + \frac{1}{R_5} + \frac{1}{R_7} + \frac{1}{R_L} \right) x_9 \right] \quad (24)$$

Now, the variable x_8 is used to force x_7 to track the desired value x_7^* given by (24). Therefore, the Lyapunov function candidate $V_7 = \frac{1}{2} (x_7 - x_7^*)^2$ is proposed. If the reference for x_8 is selected as:

$$x_8^* = -C_7 K_7 (x_7 - x_7^*) + \frac{1}{R_7} (x_7 - x_9) + C_7 \dot{x}_7^* \quad (25)$$

with $K_7 > 0$ then, $\dot{V}_7 = -K_7 (x_7 - x_7^*)^2 \leq 0$. Finally, the controller u_3 is designed to make x_8 track the desired value of (25) for x_8^* by defining:

$$u_3 = \frac{L_8}{V_s} \left(\frac{x_7}{L_8} + \frac{R_{08}}{L_8} x_8 + v_3 + \dot{x}_8^* \right) \quad (26)$$

$$v_3 = -k_{13} \text{sign}(\sigma_8) |\sigma_8|^p - k_{23} \sigma_8 + z_3 \quad (27)$$

$$\dot{z}_3 = -k_{33} \text{sign}(\sigma_8) - k_{43} (1 - \delta) \sigma_8 - \delta k_{53} z_3$$

$$z_3(0) = 0 \quad (28)$$

with $\sigma_8 = x_8 - x_8^*$ and x_8^* being given by (25). \dot{x}_8^* stands for the derivative of the reference target (25), $\delta \in \left\{ 0, \frac{1}{2}, 1 \right\}$ is

shared by all controllers and $k_{j3} > 0$ are positive gains for $j = 1, 2, \dots, 5$. Likewise, the controller (26)-(28) renders the closed-loop for the variable x_8 to:

$$\dot{\sigma}_8 = \dot{x}_8 - \dot{x}_8^* = -k_{13} \text{sign}(\sigma_8) |\sigma_8|^p - k_{23} \sigma_8 + z_3 \quad (29)$$

for which the appropriate choice for the positive gains k_{j3} allows ensuring $x_8 \rightarrow x_8^*$, which in turn ensures that $x_7 \rightarrow x_7^*$ backstepping once, and finally, guaranteeing that $x_9 \rightarrow x_9^*$ since $\dot{V}_9 \leq 0$. Consequently, the proposed controller successfully achieves the control objective set up for u_3 , which is the regulation of x_9 to the desired constant reference x_9^* regardless of the potentially time-varying and unknown load R_L . Moreover, the control signals u_1, u_2, u_3 are constrained to the interval $[0, 1]$ since they represent a duty cycle. In this way, the following saturation is included for $i = 1, 2, 3$ in the actual control command applied to the system:

$$u_i = \begin{cases} 1 & u_i > 1 \\ u_i & 0 \leq u_i \leq 1 \\ 0 & u_i < 0 \end{cases} \quad (30)$$

The overall controller structure is depicted in Figure 2.

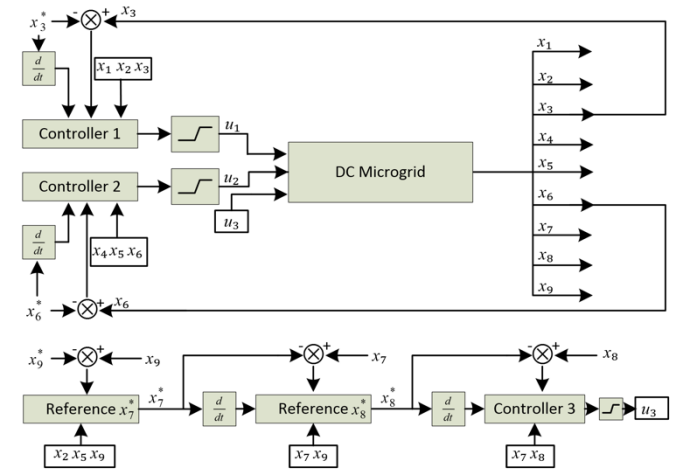


Fig. 2. Block-diagram representing the proposed controller.

Remarks. 1. The resistive load R_L appears in the control law (26) through the reference signal (24). Since R_L is unknown in general, a nominal value for it should be included in (24). It will be shown in simulation examples that the control objective is achieved regardless the mismatch between the nominal and actual value of R_L and even in the presence of time-varying behaviors. Therefore, the proposed approach merges the simplicity of the backstepping design along with the robustness properties of the super-twisting sliding mode controllers.

2. The approach adopted in this work slightly differs from the one followed in (Iovine et al., 2017) since the Lyapunov function V_9 , only contains x_9 instead of x_2, x_5, x_9 . Thus, the theoretical results are not so strong as in (Iovine et al., 2017) but the implementation of the controller is simpler and the results obtained are satisfactory, as simulation examples will show.

3. Due to the backstepping approach followed for u_3 , two derivatives (\dot{x}_7^* and \dot{x}_8^*) are needed to compute the control

command (26). This fact makes the behavior of u_3 and x_9 slightly different from the one obtained for u_1 and u_2 .

4. Notice that the control commands are composed of two parts: a feedback linearization part that cancels the coupling dynamics of the controlled variable with the others and a second part that renders it to the super-twisting structure. In this way, the interaction among state variables is avoided and each sliding control command is designed to achieve the control objective of just the controlled variable.

This work will show the effectiveness of the proposed controller and will conduct a sensitivity analysis of the closed-loop control performance when different combinations of parameters are employed.

4. SIMULATION EXAMPLES

The system described in Figure 1 and represented by Equations (1)-(9) is used for computer simulation examples where the parameters contained in Table 1 are used to describe the dynamics of the system.

Table 1. Parameters of the DC microgrid (1)-(9), (Abdali et al., 2020).

Parameters	Values	Parameters	Values	Parameters	Values
L_3	0.033H	R_7	0.1Ω	C_1	0.1F
L_6	0.033H	R_{01}	0.01 Ω	C_2	0.01F
L_8	0.0033H	R_{02}	0.01 Ω	C_4	0.1F
R_2	0.1Ω	R_{04}	0.01 Ω	C_5	0.01F
R_4	0.1 Ω	R_{05}	0.01 Ω	C_7	0.01F
R_5	0.01 Ω	R_{07}	0.01 Ω	C_9	0.0001F
V_{bus}	1000V	R_{08}	0.01 Ω	R_1	0.1 Ω

This Section is divided into two subsections: the first one is devoted to the case when there is no parameter mismatch in the system while the second one treats the case when parametric uncertainties are present.

4.1. Performance of the controller without uncertainty in converters' parameters

Initially, the effect of control gains, super-twisting index p and flag signal δ will be discussed. To this end, the signal u_1 will be employed to display and discuss the results since the effect of these parameters in the closed-loop performance is the same in all control commands. Finally, a complete simulation for the whole system will show the effectiveness of the introduced controller in a general case. The following constant parameters are used now:

$$V_B = 400 V, V_{PV} = 400 V, V_S = 1850 V, R_L = 245 \Omega, p = 0.5 \tag{31}$$

$$k_{11} = 2, k_{21} = 2, k_{31} = 4, k_{41} = 4 \tag{32}$$

The desired equilibrium point for the system is given by:

$$x_e = [300 \ 1028.2 \ 1000 \ 100 \ 1002.1 \ 3000 \ 1000 \ 0 \ 1000]^T \tag{33}$$

while the initial condition for the system is $x_0 = 1.2x_e$, i.e. the initial state of the system is 20% ahead of the desired

equilibrium point. This high mismatch allows us to show the effect of control parameters at large. The effect of δ is displayed in Figures 3 and 4.

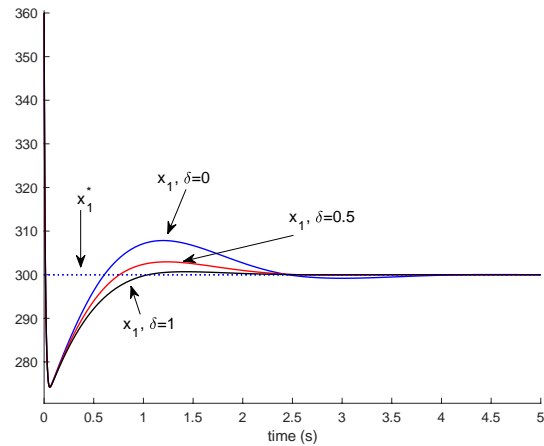


Fig. 3. Evolution of variable x_1 with the proposed controller for different values of δ .

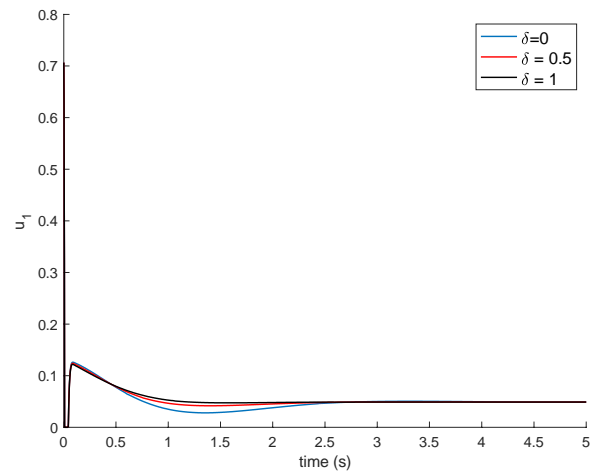


Fig. 4. Control signal u_1 associated to different values of δ .

It is deduced from Figure 3 that the control objective is achieved regardless the value of δ . However, the case corresponding to $\delta = 1$ provides the fastest response (the equilibrium point is reached the soonest) in comparison with other values of δ . This case corresponds to the situation when the regulation equation (18) does not include the value of the sliding surface. The Figure 4 displays the corresponding values for the control signal u_1 . It is observed in Figure 4 that the control signal does not experience noticeable changes with the value of δ . Consequently, it is recommended to tune the control algorithm with $\delta = 1$. Now the effect of the super twisting index p will be discussed. To this end, $\delta = 1$ is fixed, since it corresponds to the fastest behavior for the regulation equation and the remaining parameters are given by (31)-(32). The value of p will be changed. The Figures 5 and 6 depict the performance of the system in this case and display the behavior of the x_1 variable (Figure 5) and the control input u_1 (Figure 6).

It is deduced from Figures 5 and 6 that the index p plays a significant role in the closed-loop performance. As the value of p increases, the system becomes faster and exhibits

oscillations for high values of p . Anyhow, the control objective is achieved in all cases, for all values of p .

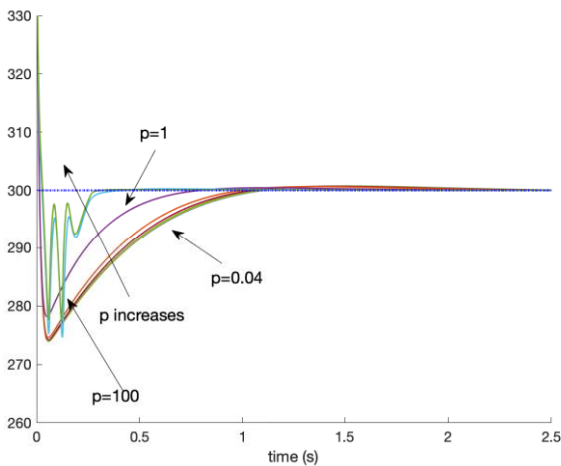


Fig. 5. Evolution of variable x_1 for different values of p and $\delta = 1$.

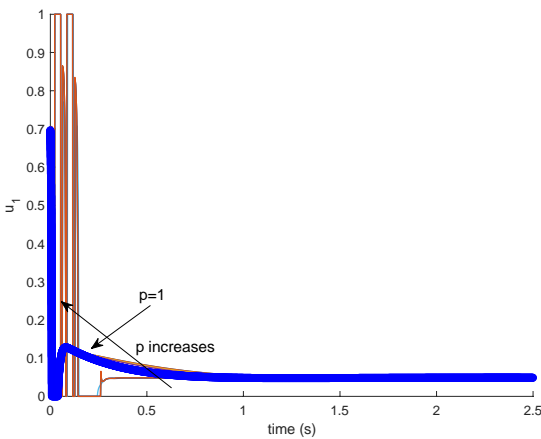


Fig. 6. Control signal u_1 for different values of p and $\delta = 1$.

The control signal varies accordingly, as it can be observed in Figure 6, and it saturates most as the value of p becomes higher. It is concluded that appropriate values for p lie in the interval $\frac{1}{5} \leq p \leq 1$. It is to point out that from a theoretical perspective, the control objective achievement is only guaranteed when $0 < p < 1$; however, higher values for p have been considered to show its effect from a simulation scenario.

The effect of control gains will be studied now. Thus, $\delta = 1$ and $p=0.5$ will be used and gains will be varied. The control gains are generated by $k_{11} = \lambda, k_{21} = \lambda, k_{31} = 2\lambda, k_{41} = 2\lambda$ so that all the gains are defined by a single parameter λ . The Figure 7 shows that the higher the control gains are, the faster the closed-loop response of the system is. It is important to notice that in all cases the control signal is chattering-free and in all cases the control objective is achieved despite it is done at different speeds. Also, the control signal does not vary too much between different control gain values. To sum up, the control recommendation is to use $\delta = 1, \frac{1}{5} \leq p \leq 1$ and higher control gains to achieve a faster closed-loop response.

Finally, a global simulation is presented to corroborate the performance of the designed controller for the whole system.

Thus, the parameters contained in Table 1 are used and the initial condition is given by $x_0 = 1.05x_e$, which corresponds to a variation of 5% from the desired equilibrium point, which is remarkable from a practical point of view. The values of $\delta = 1$ and $p=0.5$ are used while $k_{1i} = \lambda, k_{2i} = \lambda, k_{3i} = 2\lambda, k_{4i} = 2\lambda$ with $\lambda = 30$ and $k_{i3} = 100k_{i1}$ for $j = 1, 2, 3, 4$.

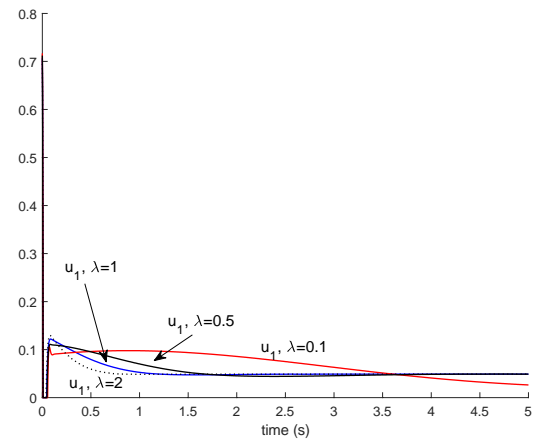
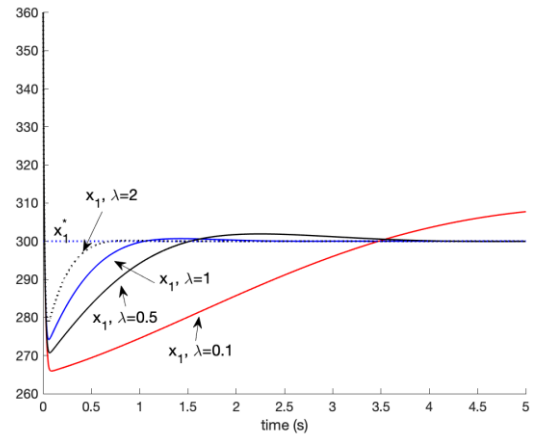


Fig. 7. Evolution of variable x_1 and corresponding control signal u_1 for different values of control gains, $p = 0.5$ and $\delta = 1$.

The gains of the third control command, the one associated to the super capacitor and designed by backstepping, are selected much higher to the gains associated to the first two control signals. This choice is made since the effect of the controller is shadowed in some way by the backstepping process and the time derivatives needed to implement the control command.

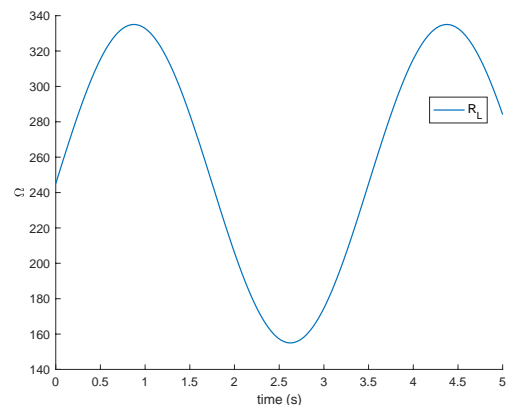


Fig. 8. Time-varying resistive load R_L .

Therefore, higher values of the gains are recommendable. Also, $K_7 = K_9 = 5$. The value of the resistive load is time-varying according to the shape portrayed in Figure 8. The nominal value is given by $R_L = 245 \Omega$. This means that the controller is tuned by using this constant value of load while the actual value is given at each time instant by the periodic variation displayed in Figure 8.

The input voltages are also time-varying and their shapes are depicted in Figure 9. The Maximum Power Point is also considered to be time-varying, as it would be in a real practical application. The Figure 10 displays the evolution of system's states under the proposed controller.

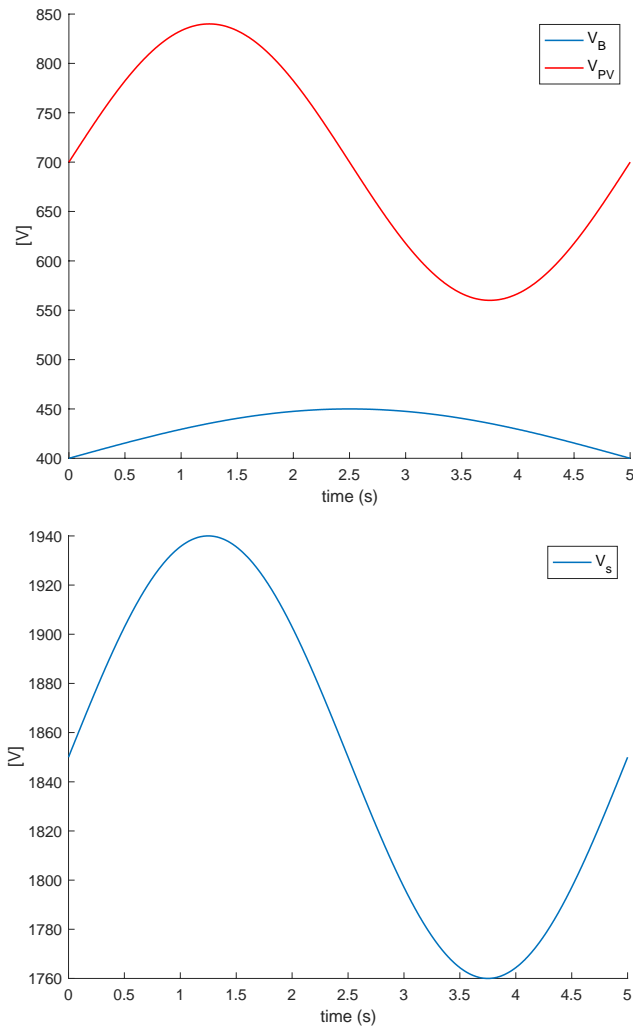
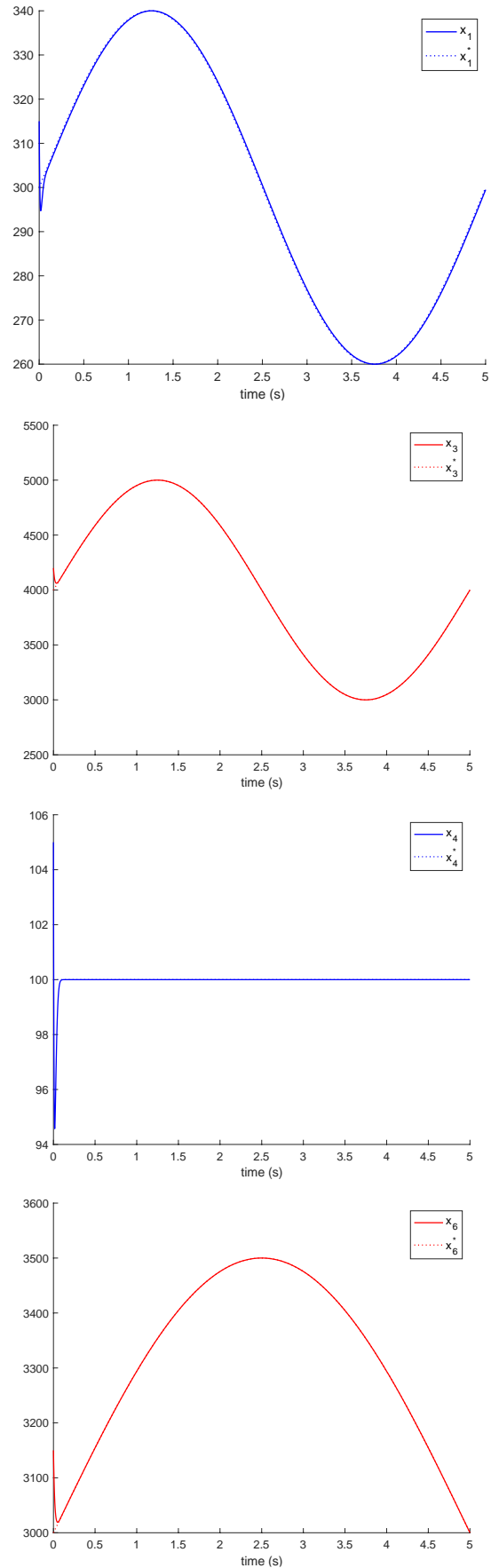


Fig. 9. Evolution of input voltages V_{PV} , V_B and V_S .

It is observed that all control objectives are fulfilled, the transient behavior vanishes very fast and the bus voltage is regulated at the desired value despite all the time-varying behaviors. It can be also deduced that the variable x_9 possesses a slower response than the variables controlled by u_1 and u_2 . This happens because the backstepping procedure shadows the effectiveness of the super-twisting controller. Therefore, the gains of the third controller should be chosen larger than the other two set of gains.



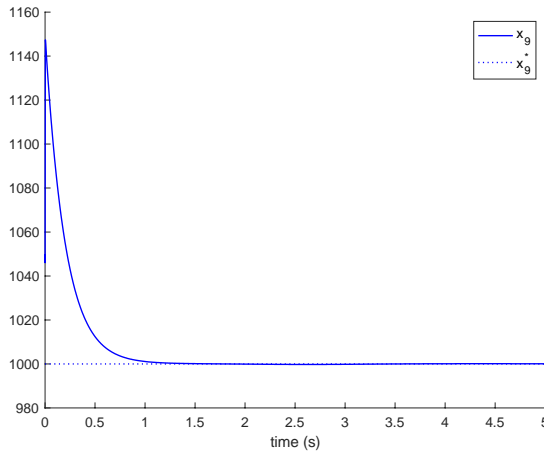


Fig. 10. Evolution of the system states with the proposed controller when the load and input voltages are given by Figures 8 and 9, respectively.

The Figure 11 displays the control commands. It is observed again that u_1 and u_2 have a different behavior than u_3 . Thus, u_1 and u_2 are chattering-free, evolve continuously with time and are smooth. On the other hand, u_3 exhibits a little ripple. This aspect is not attributable to the super-twisting controller but to the presence of the time derivatives \dot{x}_7^* and \dot{x}_8^* in the control law (26).

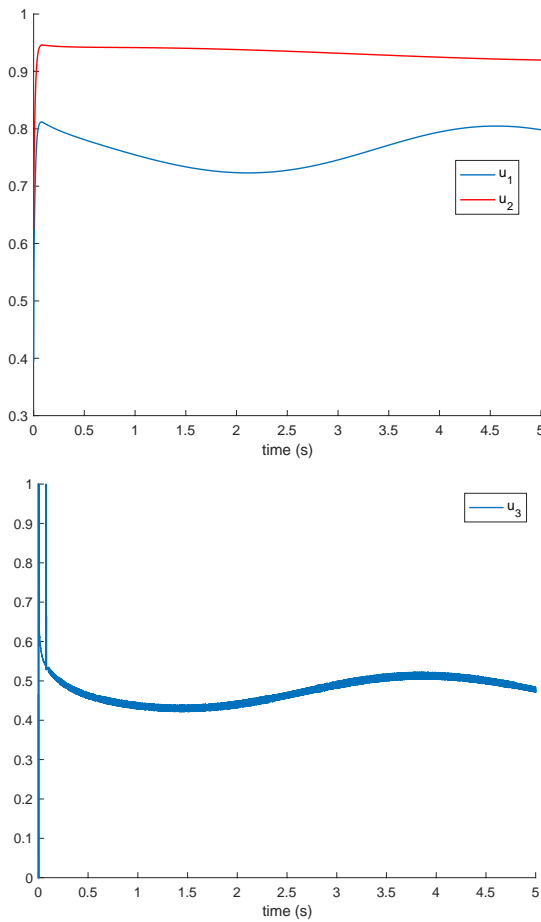


Fig. 11. Control signals obtained with the proposed controller when the load and input voltages are given by Figures 8 and 9, respectively.

However, the amplitude is small, and it does not constitute an important issue in practice. In conclusion, the proposed controller is able to achieve the desired control objective satisfactorily with a simpler design than the ones introduced in (Iovine et al., 2017) where the backstepping procedure is more involved or in (Abdali et al., 2020) where a complex state dependent Riccati equation has to be solved.

4.2. Performance of the controller under uncertainty in converters' parameters

This Section is devoted to study the effect of parameter uncertainty in the converters' components. Therefore, nominal values are used in the control laws derived in Section 3 instead of the actual values of the elements. The nominal values used for control calculation are given in Table 2 while the actual values of components are given in Table 1.

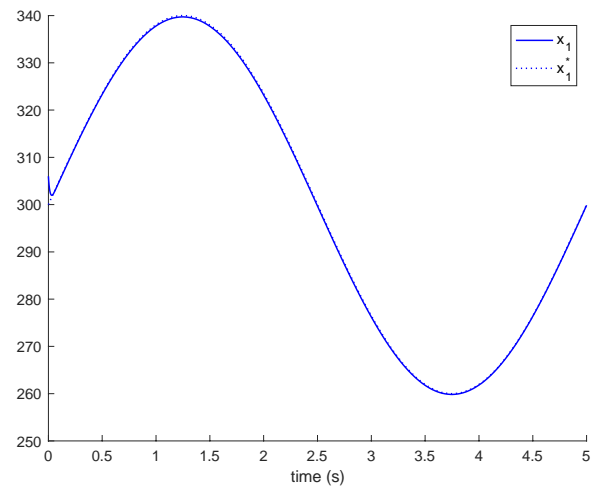
It is remarkable to notice that the values of the resistors R_1 and R_4 may be estimated from direct measurements by using the equilibrium equation (10). Consequently, the values of these resistors are estimated as:

$$\hat{R}_1(t) = \frac{V_{PV}(t) - x_1(t)}{x_3(t)}, \quad \hat{R}_4(t) = \frac{V_B(t) - x_4(t)}{x_6(t)}$$

Table 2. Nominal Parameters of the DC microgrid (1)-(9), employed in the control command calculation.

Parameters	Values	Parameters	Values	Parameters	Values
L_{3n}	0.031H	R_{7n}	0.102 Ω	C_{1n}	0.105F
L_{6n}	0.032H	R_{01n}	0.011 Ω	C_{2n}	0.0102F
L_{8n}	0.0034H	R_{02n}	0.012 Ω	C_{4n}	0.11F
R_{2n}	0.105 Ω	R_{04n}	0.0098 Ω	C_{5n}	0.011F
R_{4n}	0.099 Ω	R_{05n}	0.011 Ω	C_{7n}	0.0105F
R_{5n}	0.099 Ω	R_{07n}	0.0103 Ω	C_{9n}	0.000097F
V_{bus}	1000V	R_{08n}	0.0102 Ω	R_{1n}	0.096 Ω

These equations will be used as the values for the resistors instead of the nominal values for R_{1n} and R_{4n} . In addition, the values of K_7 and K_9 are increased to 500 in order to cope with parameters' mismatch. Figures 8 and 9 depict the evolution of load and external voltage inputs and $\delta = 1$, $p=0.5$. The results obtained are shown in Figures 12, 13 and 14.



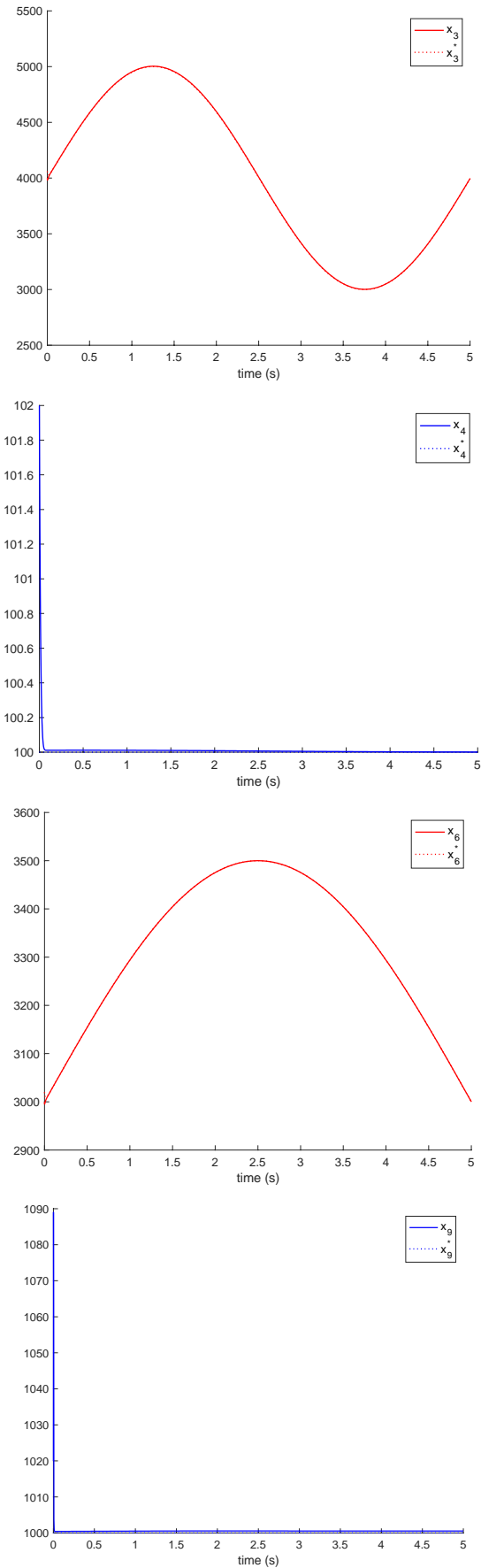


Fig. 12. Evolution of the system states with the proposed controller when the load and input voltages are given by

Figures 8 and 9, respectively, and uncertainty in converters' parameters is considered.

It can therefore be concluded that the controller is able to deal with the parametric mismatch and track the desired trajectories satisfactorily. Thus, the proposed controller achieves the control objective adequately in a wide variety of situations.

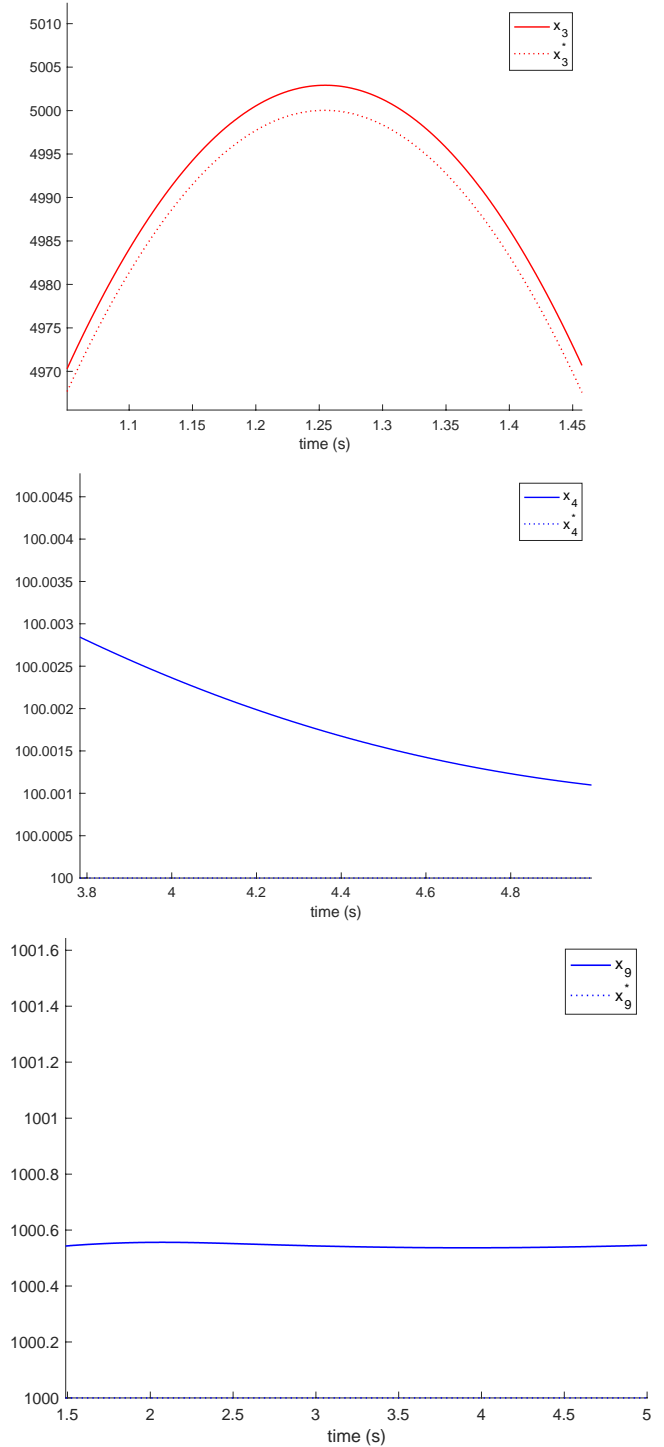


Fig. 13. Zoom on the Figure 12.

5. CONCLUSIONS

This work is devoted to the design of a robust super-twisting sliding mode controller for a DC microgrid integrating a photovoltaic source, a supercapacitor and a battery. A

capacitor is added on the source side so that the system is not fully controllable while the voltage at this capacitor is controlled instead, guaranteeing thus the regulation of the grid voltage. This is a common practice in real systems. The system is controlled by means of three control signals.

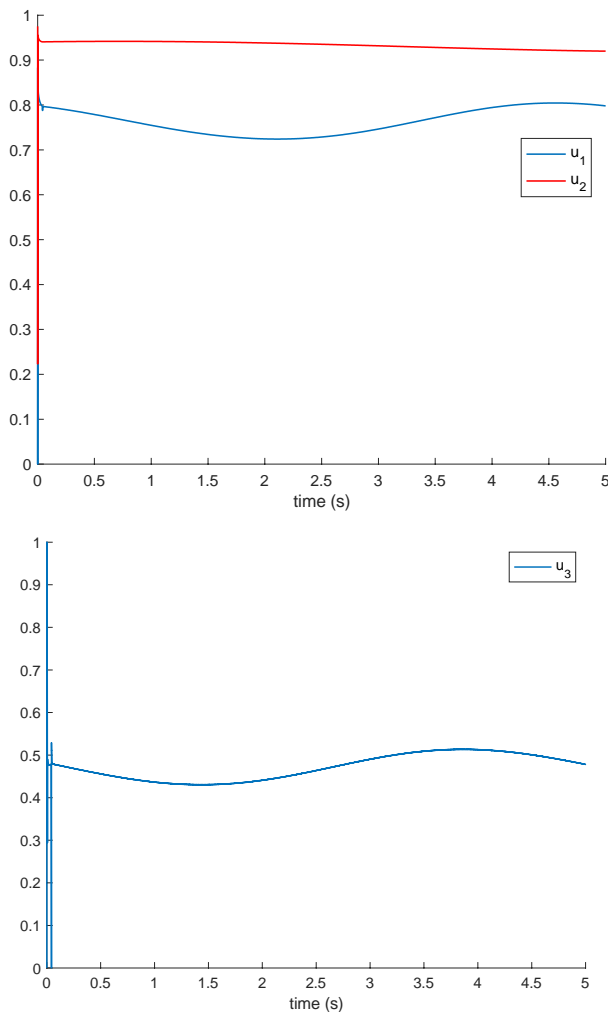


Fig. 14. Control signals obtained with the proposed controller when the load and input voltages are given by Figures 8 and 9, respectively, and uncertainty in converters' parameters is considered.

The super-twisting controller can be directly designed for the first two control signals but a backstepping methodology is merged with the super-twisting technique for the third one, controlling the bus capacitor voltage. This approach allows taking advantage of the simplicity of the backstepping method while ensuring the robustness of the system with respect to changes in the resistive load. As simulation examples have shown, the controller is able to guarantee the tracking control of desired variables even when the load is changing in time. A sensitivity analysis is conducted on the parameters of the system revealing the influence of the controller free-design parameters in the performance of the closed-loop system. The super-twisting index is recommended to be selected in the range $\frac{1}{5} \leq p \leq 1$, the regulation signal is recommended to be $\delta = 1$ while the higher the control gains are, the faster the closed-loop response is. In addition, the control gains

corresponding to the third control signal are recommended to be selected much higher than the gains of the other two to overcome the shadowing caused by the backstepping procedure and the calculation of the derivatives involved in the determination of u_3 . It has also been shown that the controller is able to obtain an acceptable performance when parametric uncertainty is present in the system. Overall, the proposed scheme can achieve the control objectives satisfactorily and in a much simpler way than previous works. As a future work, the proposed control algorithms will be implemented and tested in real laboratory platforms.

ACKNOWLEDGEMENTS

This work was supported by the Research Groups Program funded by Deanship of Scientific Research, Taif University, Ministry of Education, Saudi Arabia, under Grant 1-441-106. The authors would like to thank anonymous reviewers for their helpful comment that have helped improve the quality of the paper.

REFERENCES

- Abdali, A., Mazlumi, K. & Guerrero, J.-M. (2020). Integrated Control and Protection Architecture for Islanded PV-Battery DC Microgrids: Design, Analysis and Experimental Verification. *Applied Sciences* 2020, 10, 8847.
- Alharbi, Y.M., Al Ahmadi, A.A., Ullah, N., Abeida, H., Soliman, M.S. & Khraisat, Y.S.H. (2020). Super twisting Fractional Order Energy Management Control for a Smart University System Integrated DC Micro-Grid. *IEEE Access*, vol. 8, pp. 128692-128704.
- Alzain O. B., Liu X., King X. (2021). Optimized Sliding Mode Regulation based on Particle Swarm Optimization Algorithm for Non-Linear DFIG-Wind Turbine, *Control Engineering and Applied Informatics*, vol. 23, no. 4, pp. 33-45.
- Badal, F.R., Das, P., Sarker, S.K. & Das, S.K. (2019). A survey on control issues in renewable energy integration and microgrid. *Protection and Control of Modern Power Systems* (2019) 4:8.
- Cai, H., Hu, G., Lewis, FL & Davoudi, A. (2016). A distributed feedforward approach to cooperative control of ac microgrids. *IEEE Trans Power Syst* 2016;31(5):4057-67.
- Cho, H. & Kerschen, G. (2016). Simple Adaptive Methodology for Chattering-free Sliding Mode Control. *Proceedings of the 2016 14th International Workshop on Variable Structure Systems (VSS)*, Nanjing, China, pp. 280-285.
- Cucuzzella, M., Lazzari, R., Trip, S., Rosti, S., Sandroni, C. & Ferrara, A. (2018). Sliding mode voltage control of boost converters in DC microgrids. *Control Engineering Practice* 73, pp. 161-170.
- Cupelli, M., Moghimi, M., Riccobono, A. & Monti, A. (2014). A comparison between synergetic control and feedback linearization for stabilizing mvdc microgrids with constant power load. *Innovative smart grid technologies conference Europe (ISGT-Europe), 2014 IEEE PES. IEEE; 2014. p. 1-6.*

- Emelyanov, S.V., Korovin, S.K. & Levant, A. (1996). High-order sliding modes in control systems, *Computational Mathematics and Modeling*, Vol.7(3), p.294-318.
- Fekih, A., Mobayen, S. & Chen, C.-C. (2021). Adaptive Robust Fault-Tolerant Control Design for Wind Turbines Subject to Pitch Actuator Faults. *Energies* 2021, 14, 1791.
- Feng, Z. & Fei, J. (2018). Design and analysis of adaptive Super-Twisting sliding mode control for a microgyroscope. *Plos One* 13(1):e0189457.
- Gambhire, S.J., Ravi Kishore, D., Londhe, P.S. & Pawar, S.N. (2021). Review of sliding mode based control techniques for control system applications. *International Journal of Dynamics and Control* 9:363-378.
- Han, H., Liu, Y., Sun, Y., Su, M. & Guerrero, J.M. (2015). An improved droop control strategy for reactive power sharing in islanded microgrid. *IEEE Trans. Ind. Electron.* 2015, 30, 3133-3141.
- Han, Y., Ma, R. & Cui, J. (2018). Adaptive Higher-Order Sliding Mode Control for Islanding and Grid-Connected Operation of a Microgrid. *Energies* 2018, 11, 1459.
- Iovine, A., Siad, S. B., Damm, G., De Santis, E. & Di Benedetto, M. D. (2017). Nonlinear Control of a DC MicroGrid for the Integration of Photovoltaic Panels. *IEEE Transactions on Automation Science and Engineering*, vol. 14, no. 2, pp. 524-535.
- Itkis, U. (1976). Control systems of variable structure, Wiley, New York.
- Jouini, M., Dhahri, S. & Sellami, A. (2017). Design of Robust Supertwisting Algorithm Based Second-Order Sliding Mode Controller for Nonlinear Systems with Both Matched and Unmatched Uncertainty. *Complexity* 2017:1972921, 8 pages.
- Kim, J., Guerrero, JM, Rodriguez, P., Teodorescu, R. & Nam, K. (2011). Mode adaptive droop control with virtual output impedances for an inverter-based flexible ac microgrid. *IEEE Trans Power Electron* 2011;26(3):689-701.
- Kumar, M, Srivastava, S. & Singh, S. (2015). Control strategies of a DC microgrid for grid connected and islanded operations. *IEEE Trans Smart Grid* 2015;6(4):1588-601.
- Levant, A., (2001). Universal single-input-single-output (SISO) sliding-mode controllers with finite-time convergence, *IEEE Trans. on Aut. Contr.*, Vol. 46, no. 9, pp. 1447-145.
- Lu, X., Guerrero, JM., Sun, K. & Vasquez, JC. (2014). An improved droop control method for dc microgrids based on low bandwidth communication with DC bus voltage restoration and enhanced current sharing accuracy. *IEEE Trans Power Electron* 2014;29(4):1800-12.
- Mobayen, S., Bayat, F., Lai, C.-C., Taheri, A. & Fekih, A. (2021). Global Sliding Mode Controller Design for Perturbed DC-DC Buck Converters. *Energies* 2021, 14, 1249.
- Mohamed, YA-RI, Zeineldin, HH, Salama, M & Seethapathy, R. (2012). Seamless formation and robust control of distributed generation microgrids via direct voltage control and optimized dynamic power sharing. *IEEE Trans Power Electron* 2012;27(3):1283-94.
- Mondal, S. & Mahanta, C. (2013). Chattering free adaptive multivariable sliding mode controller for systems with matched and mismatched uncertainty. *ISA Transactions* 52:335-341.
- Moreno, J.A. (2014). On strict Lyapunov functions for some non-homogeneous super-twisting algorithms. *Journal of the Franklin Institute* 351:1902-1919.
- Nagesh, I. & Edwards, C. (2014). A multivariable super-twisting sliding mode approach. *Automatica* 50, 3:984-988.
- Pati, A.K. & Sahoo, N.C. (2017). Adaptive super-twisting sliding mode control for a three-phase single-stage grid-connected differential boost inverter based photovoltaic system. *ISA Transactions* 69 (2017), pp. 296-306.
- Sami, I., Ullah, S., Ali, Z., Ullah, N. & Ro, J.-S. (2020). A Super Twisting Fractional Order Terminal Sliding Mode Control for DFIG-Based Wind Energy Conversion System. *Energies* 2020, 13, 2158.
- Sami, I., Ullah, S., Ali, Z., Ullah, N. & Ro, J.-S. (2021). Sensorless fractional order composite sliding mode control design for wind generation system. *ISA Transactions*. Vol. 111, pp. 275-289.
- Sarkar, P., Hazra, A. & Mondal, A. (2020). A unified approach for PI controller design in delta domain for indirect field-oriented control of induction motor drive. *Journal of Engineering Research* 8, 3:118-134.
- Setyawan, L., Peng, W. & Jianfang, X. (2014). Implementation of Sliding Mode Control in DC Microgrids. 2014 9th IEEE Conference on Industrial Electronics and Applications. 9-11 June 2014. Hangzhou, China.
- Shen, H., Iorio, J. & Li, N. (2019). Sliding Mode Control in Backstepping Framework for a Class of Nonlinear Systems. *J. Mar. Sci. Eng.* 2019, 7, 452.
- Siddiqui, M.A., Anwar, M.N., Shamsuzzoha, M. & Mahboob, M.R. (2020). Closed Loop Tuning of Cascade Controllers Based on Setpoint Experiment. *Journal of Engineering Research* 8, 4:117-138.
- Stojic, D. (2021). Modified Single-Phase Adaptive Transfer Delay Based Phase-Locked Loop with DC Offset Compensation, *Control Engineering and Applied Informatics*, vol. 23, no. 2, pp. 23-31.
- Svecko, R., Gleich, D. & Sarjas, A. (2020). The Effective Chattering Suppression Technique with Adaptive Super-Twisted Sliding Mode Controller Based on the Quasi-Barrier Function: An Experimentation Setup. *Applied Sciences* 2020, 10, 595.
- Tayebi-Haghighi, S., Piltan, F. & Kim, J.-M. (2018). Robust composite high-order super-twisting sliding model control of robotic manipulators, *Robotics*, 2018, 7, 13.
- Tobón, A., Peláez-Restrepo, J., Montano, J., Durango, M., Herrera, J. & Ibeas, A. (2020). MPPT of a Photovoltaic Panels Array with Partial Shading Using the IPSM with Implementation Both in Simulation as in Hardware. *Energies* 2020, 13, 815.
- Ullah, N. (2020). Fractional Order Sliding Mode Control Design for a Buck Converter Feeding Resistive Power Loads. *Mathematical Modelling of Engineering Problems* 7, 4:649-658.

- Utkin, V. I. (1977). Variable structure systems with sliding modes, *IEEE Trans. on Aut. Control*, vol. AC-22, pp. 212-222.
- Weng, S., Yue, D., Dou, C., Shi, J. & Huang, C. (2019). Distributed event-triggered cooperative control for frequency and voltage stability and power sharing in isolated inverter-based microgrid, *IEEE Transactions on Cybernetics*, vol. 49, no. 4, pp. 1427-1439.
- Xu, L. & Chen, D. (2011). Control and operation of a DC microgrid with variable generation and energy storage. *IEEE Transactions on Power Delivery* 26:2513–2522.
- Zeb, K., Busarello, T.D.C., Ul Islam, S., Uddin, W., Raghavendra, K.V.G., Khan, M.A. & Kim, H.-J. (2020). Design of Super Twisting Sliding Mode Controller for a Three-Phase Grid-connected Photovoltaic System under Normal and Abnormal Conditions. *Energies* 2020, 13, 3773.
- Zhang, L., Chen, K., Chi, S. Lyu, L. & Cai, G. (2019). The hierarchical control algorithm for DC microgrid based on the improved droop control of fussy logic, *Energies*, 2019, 12, 2995.
- Zhang, Q., Zhuang, X., Liu, Y., Wang, C. & Guo, H. (2019). A novel autonomous current-sharing control strategy for multiple paralleled DC-DC converters in islanded DC microgrid, *Energies*, 2019, 12, 3951.
- Zhang, D. & Wang, J. (2017). Adaptive Sliding-Mode Control in Bus Voltage for an Islanded DC Microgrid, *Mathematical Problems in Engineering*, Volume 2017, Article ID 8962086, 9 pages.